System identification and microposition control of ionic polymer metal composite for three-finger gripper manipulation

Kwansoo Yun and **Won-jong Kim***
Department of Mechanical Engineering, Texas A&M University, Texas, USA

The manuscript was received on 27 October 2005 and was accepted after revision for publication on 30 May 2006.

DOI: 10.1243/09596518JSCE215

Abstract: Smart materials have been widely used for control actuation. A robotic hand can be equipped with artificial tendons and sensors for the operation of its various joints, mimicking human hand motions. The motors in the robotic hand could be replaced with novel electroactive polymer (EAP) actuators. In the three-finger gripper proposed in this paper, each finger can be actuated individually so that dexterous handling is possible, allowing precise manipulation. To develop model-based control laws, an approximated linear model representing the electromechanical behaviour of the gripper fingers is introduced. Several chirp voltage signal inputs were applied to excite the IPMC (ionic polymer metal composite) actuators in the interesting frequency range of (0.62 Hz, 5 Hz) for 30 s at a sampling frequency of 250 Hz. The linear Box–Jenkins (BJ) model was well matched with the model obtained using a stochastic power spectral method. With feedback control, the large overshoot, rise time, and settling time associated with the inherent material properties were reduced. The motions of the IPMC fingers in the microgripper would be coordinated to pick, move, and release a macro- or micro-part. The precise manipulation of this three-finger gripper was successfully demonstrated with experimental closed-loop responses.

Keywords: IPMC, actuator, sensor, BJ model, position control, digital PID controller, LQR

1 INTRODUCTION

Microgrippers are essential tools in industrial processes. An integrated microgripper system, which can be easily implemented with any platforms operated with the objects having a wide range of sizes and shapes, will have a great impact on micro-optics manipulation, microelectromechanical systems (MEMS), fibre-optics assembly, biomedical manipulation, and semiconductor manufacturing. The success of microgrippers heavily depends on the reliability and durability of the actuator and the sensor. The main goal of this paper is to develop and implement a new generation of precision position control with a smart three-finger gripper system that would enhance manipulation capabilities and add intelligence to existing systems with regard to design, performance, and cost. This research is aimed at achieving this goal by meeting the following objectives:

(a) to improve the ionic polymer metal composite (IPMC)-based actuator and sensor performance with a linearized model by increasing its dynamic range and making it less sensitive to measurement noise.
(b) to develop multivariable control schemes and implement them in real-time applications.
(c) to operate a three-finger gripper with proper functioning, repeatability, and reliability.

In the last decade a new class of polymers has emerged that responds to external electrical stimulation by exhibiting significant shape or size change. Electroactive polymers (EAPs) attracted much attention from diverse disciplines. The typical two types of base polymers are employed to form

* *Corresponding author: Department of Mechanical Engineering, Texas A&M University, 3123 TAMU, College Station, TX 77843-3123, USA. email: wjkim@tamu.edu*

IPMCs. These are Nafion® (perfluorosulphonate manufactured by DuPont) and Flemion® (perfluorocaboxylate manufactured by Asahi Glass, Japan). Nemat-Nasser and Wu [**1**] compared the Nafion-based IPMC with the Flemion-based IPMC as a substitute for a bending actuator. Shahinpoor and Kim reported the effects of the surface electrode (platinum) resistance depositing a thin layer of silver on top of the platinum electrode to improve the performance of IPMC [**2**] and found out the IPMC having Li^+ had the best performance in terms of force generation among other cations [**3**]. In general, the electrolysis occurring within the membrane causes the degradation of the IPMC, i.e. dehydration and loss of conductivity in surface electrodes. To prevent this degradation from the electrolysis, the low-temperature condition helped reduce the rate of degradation [**4**]. On the other hand, the freeze-dried IPMC sample was used to enhance the electromechanical properties since it increased the storage of free water, allowing more effective diffusion [**5**]. Kim and Shahinpoor [**6**] increased the IPMC thickness up to 2 mm by adding more electroactive polymer and ion-conducting powder with electroactive polymer to enhance force generation.

This research focuses on the design of a miniature displacement mechanism and the electromechanical characteristics of an IPMC actuator. Strips of EAP composites can bend and flap dramatically when an electric voltage is applied. In this sense they are large motion actuators; they can move and exert force. Conversely, when a strip is bent, a voltage is produced across its thickness, allowing the strip to behave like a sensor that can determine a given level of force and motion [**7**], with the possible measurement of the generated voltage on the order of millivolts. These are EAPs that bend in response to an electrical activation as a result of the mobility of cations in the polymer network. IPMC requires relatively low voltages (1–10 V) to generate bending responses at low frequencies below 1 Hz.

Since micromechanical systems such as micro-optical devices, microfluidic components, or other hybrid microsystems became ever more complex, developing an enabling microassembly technique is of great importance. The production of microsystems requires a tighter control due to the small size of the microparts to be mounted in hybrid microsystems (e.g. microlenses, optical fibre, and microtubes). It also needs very high accuracy in the assembly processes, which cannot be achieved with conventional assembly equipment. Therefore the demand of microassembling tools as high-precision robots and microgrippers has increased dramatically.

Ionic polymer actuators were modelled in various ways by taking relevant physical phenomena into consideration. Electromechanical modelling was performed with an Euler–Bernoulli beam theory. The governing equation used in reference [**8**] assumed a small bending deflection. Actual bending deflections can be large, which is contradictory to this assumption. The material properties of IPMC were not fully considered in references [**9**] and [**10**] since the measurement of the deflection of the activated IPMC strip is related to its Young's modulus because the Young's modulus of IPMC is a function of frequency and temperature [**11**]. Nemat-Nasser and Li [**12**] developed a model accounting for the coupled ion transport, electric field, and elastic deformation to predict the response of the Nafion-based IPMC.

The Kanno–Tadokoro model contains the electrical, stress generation, and mechanical stages [**13**]. For the electrical model, the characteristic is approximated by a series connection of RC circuits based on an experimental curve. In the stress generation stage, the internal stress playing a key role in bending was represented by a similar manner of piezoelectric elements. Shahinpoor [**14**] applied the theoretical model of IPMC using linear irreversible thermodynamics for IPMC actuation and sensing phenomena. Paquette *et al.* [**15, 16**] updated the Kanno–Tadokoro model by adding linear irreversible thermodynamics to improve its robustness and coupling capabilities and expanded to the multilayer configuration.

Kim *et al.* [**17**] developed a wireless biomimetic tadpole microrobot using IPMC actuators. The undulatory motion of the fin tail using IPMC was controlled by changing the frequency and input voltage while considering the drag force. Bonomo *et al.* [**18**] developed an RLC electric circuit model including diodes and identified parameters of the model using the least-squares method. Bhat and Kim [**19**] have successfully performed a novel hybrid force and position control using a lead-lag controller and promised practical micromanipulation applications of the IPMC actuator.

The enhancement of the actuation capability of IPMC materials is studied in this paper on a fundamental level using black-box model approaches. The large strain response of IPMC to electrical simulation is non-linear and still requires adequate analytical methods for the design and control of related devices based on the material. The origin of the electroactivity in IPMC materials must be understood better to improve their performance and to offer effective design methods to enhance their robustness. The development of a dynamic model of

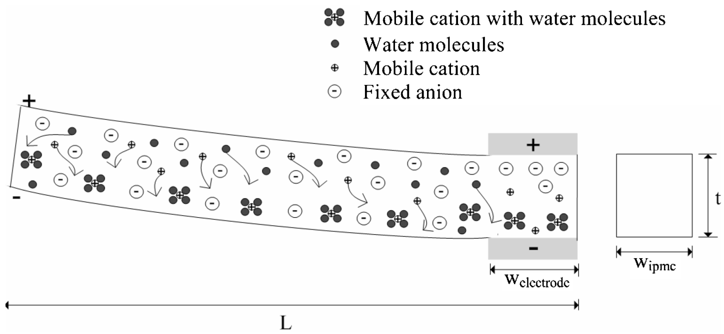

Fig. 1 Redistribution of charges in an ionic polymer due to an imposed electric field

a single-degree-of-freedom mechanism by system identification is necessary in order to design the control system to manipulate the IPMC strips in a three-finger gripper simultaneously.

This paper is organized as follows. Section 2 provides the overview of the IPMC actuator that was developed. Section 3 presents the system identification result for its plant model. The model was constructed using a Box–Jenkins (BJ) method. Section 4 describes the design of the position controller and section 5, the manipulation of a three-finger gripper motion. In section 6, simulated and experimental results obtained using the closed-loop position controller implemented on the IPMC three-finger gripper are presented.

2 WORKING PRINCIPLE OF AN IPMC ACTUATOR AND EXPERIMENTAL SET-UP

IPMC is made of a perfluorinated membrane (i.e. all of the hydrogen atoms attached to carbon atoms are replaced with fluorine atoms) with noble metal plating (typically gold or platinum) for electrodes [**20**]. The samples of the IPMCs used in this research have two metal coatings on the Nafion membrane. The first metal coating consists of many small platinum particles dispersed inside the surface of the membrane within the polymer. The depth of penetration is usually 10–20 μm. The second metal coating is gold deposited by electroplating. This coating is intended to enhance the surface conductivity of the IPMC [**7**, **21**].

Ionic polymers are typically either Flemion (a perfluorocarboxylate) or Nafion (a perfluorosulphonate) that swell in water due to their ionic and hydrophilic nature. Anions are located on the polymer membrane while cations are present and freely moving in the fluid. When an electric field is applied to the IPMC, the cations diffuse towards the negative electrode, which causes the composite polymer to deform [**7**], as depicted in Fig. 1. On the other hand, when a mechanical load is applied to the IPMC, a few millivolts are generated across the electrodes [**7**].

Typically, the strip of the perfluorinated ionic polymer membrane bends towards the anode in the case of cation exchange membranes under the influence of an electric potential. The appearance of water on the surface of the expansion side and the disappearance of water on the surface of the contraction side are common. This electrophoresis-like internal ion-water movement is responsible for creating effective deformation for actuation. Water leakage through the porous platinum electrode reduces the electromechanical conversion efficiency [**7**]. This can support the phenomenon of generating the water on the surface of the IPMC strip stuck to the negative electrode.

Figure 2 is a photograph of the experimental set-up. The IPMC strips were cut in the dimension of 25.18 mm × 4.24 mm × 0.18 mm. Laser distance sensors (Model OADM 20I44/404790 from Baumer Electronic) with a resolution of 5 μm and a position noise standard deviation of 10 μm measure the tip displacements of the IPMC fingers. This position measurement is fed to a 16-bit analogue-to-digital (A/D) converter of a floating-point digital signal processing (DSP) board (Model DS1102 from dSPACE).

Fig. 2 Photograph of the three-finger gripper

This DSP board communicates with a Pentium III personal computer for the user interface. The control voltage to actuate the IPMC strip is generated through a 16-bit digital-to-analogue (D/A) converter channel of the DSP board.

The three-finger gripper consists of three strips of IPMC clamped by cooper electrodes. Each IPMC strip can be controlled individually and approach the target object independently. One of the IPMC strips can work as a switch since the IPMC itself generates the voltage output when mechanically touched by the object. This IPMC strip can tell when the force control is required to start so that the three-finger gripper can grip the target object without damage. Figure 3 shows a schematic cross-sectional view of this three-finger gripper. The object denoted with a circle has a radius r and the three fingers around it move within the controlled range l independently. The width w can be modified to be a wedge when very small-sized objects need to be handled.

3 SYSTEM IDENTIFICATION EXPERIMENTS

In this section, a linearlized dynamic model of the IPMC actuator by system identification is presented. Because of their importance, non-linear characteristics in IPMC actuation have been studied recently. Shahinpoor and Kim [**7**] represented IPMC behaviours with small hysteresis. The particle electrodes on the IPMC surface primarily affected its hysteretic behaviour [**15**]. Kothera and Leo presented non-linear distortion using the Volterra series [**22**] and studied the closed-loop bandwidth of the cantilever actuator in both clamped–free and clamped–clamped boundary conditions [**23**]. A systematic methodology is developed in this paper to deal dexterously with the inherent non-linear behaviours of IPMC with a linearized model. Also provided is a means for system identification to improve the accuracy and reliability of IPMC actuators and sensors.

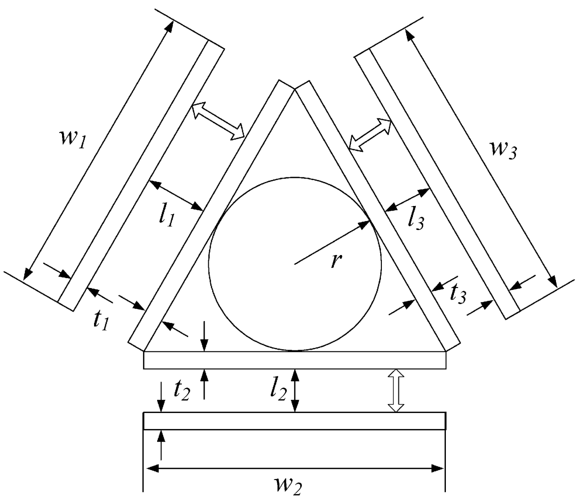

Fig. 3 Schematic cross-sectional view of the three-finger gripper

Incidentally, IPMC does not exhibit a high bandwidth for actuator applications. At high frequencies (5–20 Hz) its moduli are larger and displacements are smaller. Whereas at low frequencies mobile cations with water have time to effuse out of the surface electrodes, they are rather contained inside the base polymer (Nafion 117) at high frequencies. Therefore, the inherent behaviour of water and the ion transportation within the IPMC affect the moduli differently at various frequencies [**7**]. Thus, using IPMC at high frequencies is disadvantageous in achieving high efficiency.

A chirp signal response offers the control of both the amplitude and the frequency range of the input [**24**]. The dwelling time and the frequency interval are the keys to control the degree of dynamic equilibrium [**25**]. A chirp signal input was used to excite the actuator in the interesting frequency range of (0.62 Hz, 5 Hz) for 30 s at a sampling frequency of 250 Hz. Figure 4 shows the fast Fourier transform (FFT) magnitudes of the chirp signal inputs and the measured outputs at the interesting frequency range. The several different magnitudes of the chirp signal shown in Fig. 4(a) were applied to determine how significant the non-linear behaviour of the system would be. The parametric identification representing the system model was based on the best fit of the input–output data. If the reference input has strong enough frequency components, the estimated parameters will converge in this range [**26**].

Bhat and Kim [**19**] originally employed the saturation limit of ± 2 V to avoid the integrator windup effect, and Yun and Kim [**27**] extended the saturation limit to ± 3 V with an antiwindup scheme. As the non-linear behaviour in IPMC was defined as being due to the saturation effect [**18**, **27**], the amplitude of the chirp signal input was intentionally limited to 3 V. The output magnitudes shown in Fig. 4(b) decrease with respect to the frequency and also in terms of the applied voltages, as expected. The frequency-domain peak magnitudes of the IPMC responses to the 3, 2, and 1 V chirp signal inputs were about 0.021, 0.0175, and 0.014 mm s respectively. The frequency-domain peak magnitudes decreased by about 0.0035 mm s as the voltage magnitudes decreased by 1 V. This phenomenon might indicate that the IPMC behaviour is not highly non-linear in

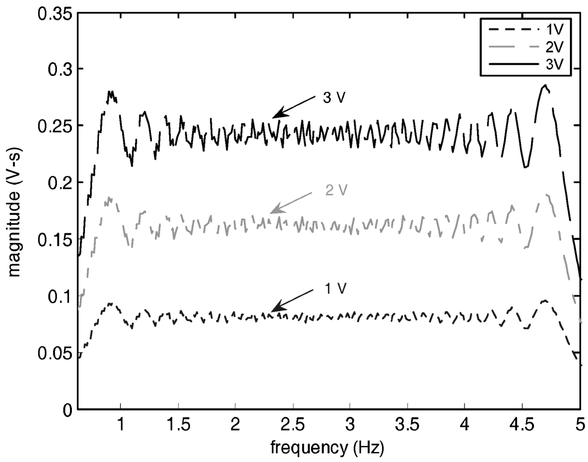

(a)

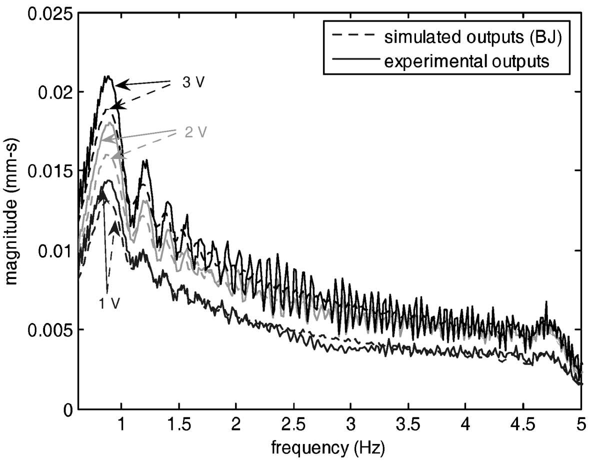

(b)

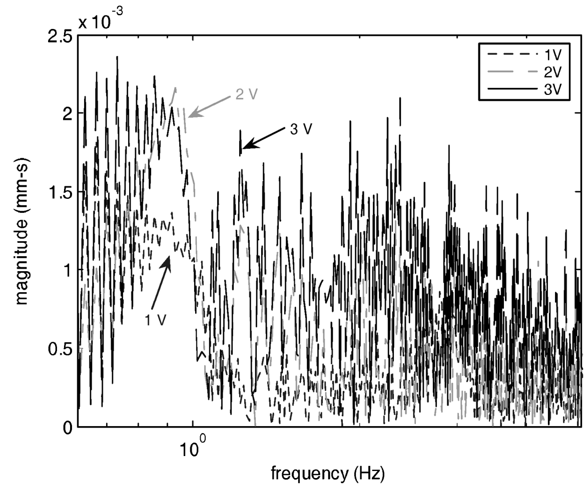

(c)

Fig. 4 (a) FFT magnitudes of the chirp signal inputs with three different input voltage magnitudes (1, 2, and 3 V). (b) FFT magnitudes of the measured displacements between the simulated outputs obtained using a BJ model and the experimental outputs. (c) Errors between the simulated outputs obtained using a BJ model and the experimental outputs

this frequency range. The average magnitude errors of the chirp signal responses are approximately 0.5 μm s, as shown in Fig. 4(c). Various discrete-time IPMC models acquired by BJ models are easily described by the rational transfer function $G(s)$ for the continuous-time system using numerator and denominator coefficients varying independently in prescribed intervals

$$G(s) = \frac{n_3 s^3 + n_2 s^2 + n_1 s + n_0}{s^4 + d_3 s^3 + d_2 s^2 + d_1 s + d_0} \tag{1}$$

where

$n_3 \in [1.207, 7.208]$, $n_2 \in [1906, 2299]$

$n_1 \in [2.04\text{e}+5, 9.816\text{e}+5]$

$n_0 \in [4.32\text{e}+5, 1.355\text{e}+7]$

$d_3 \in [22.66, 500.3]$, $d_2 \in [2.068\text{e}+5, 6.805\text{e}+5]$

$d_1 \in [1.932\text{e}+6, 1.602\text{e}+7]$

$d_0 \in [5.109\text{e}+5, 3.266\text{e}+7]$

Another way to find the transfer function of the IPMC is by using the power spectral density (PSD) analysis with the relationship

$$\Phi_{yy}(\omega) = |W(\mathrm{j}\omega)|^2 \Phi_{xx}(\omega) \tag{2}$$

where $\Phi_{xx}(\omega)$ and $\Phi_{yy}(\omega)$ are the power spectral densities of the input and the output respectively, and $W(\mathrm{j}\omega)$ is the system transfer function [**28**]. Each Bode plot of the transfer function shown in Fig. 5 exhibits a similar trend in the characteristics of the system. The system transfer function is only considered below 5 Hz, which is the interesting frequency range.

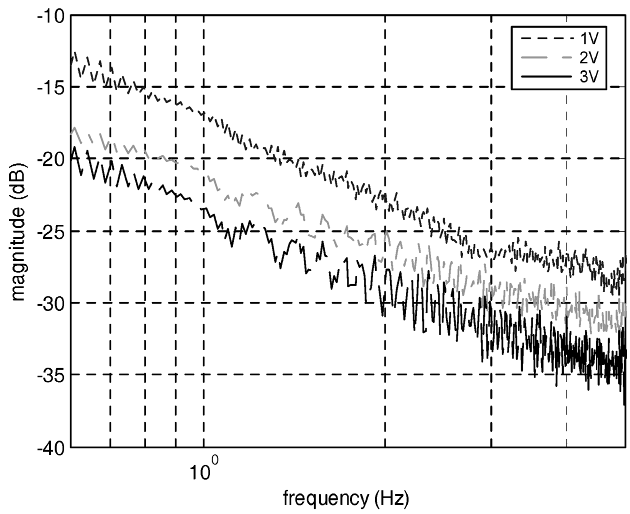

Fig. 5 Bode plots of the transfer function using a PSD analysis

Figure 6 shows that the Bode plots of the system transfer function (solid lines) obtained from the PSD analysis and those from the BJ model (dashed lines) match very well within the interesting frequency range. Figures 6(a), (b), and (c) represent the cases of the magnitudes of the chirp signal inputs of 1, 2, and 3 V respectively. From the plots shown in Fig. 6, it is concluded that the IPMC characteristics closely follow the linear BJ model in this frequency range.

4 CONTROLLER DESIGN

4.1 Proportional-integral-derivative control

As mentioned earlier, IPMC strips are used for the fingers in a three-finger gripper. Figure 7 shows the schematic diagram of the closed-loop position control of the three-finger gripper. The three-finger gripper was manipulated simultaneously by developing closed-loop controllers. The control objectives are (a) to have a 60° phase margin, (b) to follow step position commands with no steady-state error, and (c) to minimize the settling time. To achieve these control objectives, a discrete-time proportional-integral-derivative (PID) controller was designed for the IPMC gripper. First, Simulink response optimization provides a means to tune parameters within a Simulink model to meet the time-domain performance requirements [**29**]. It automatically converts time-domain constraints into a constrained optimization problem and then solves the problem using optimization routines taken from the optimization toolbox or the genetic algorithm and direct search toolbox [**29**].

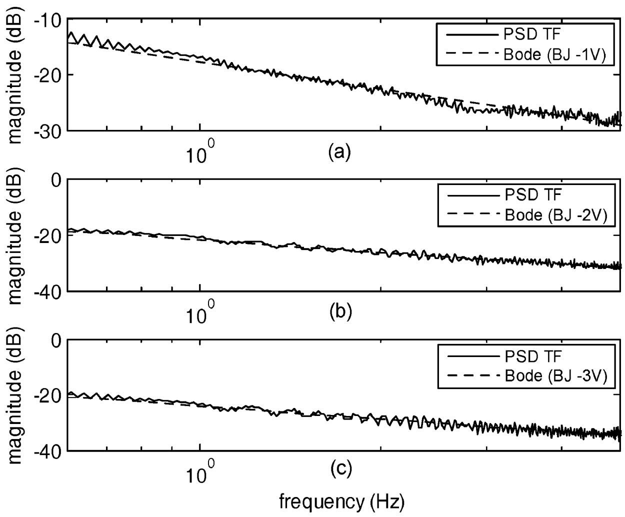

Fig. 6 Comparison of the Bode plots of the transfer function obtained from the PSD analysis (solid lines) with those from the BJ model (dashed lines). (a), (b), and (c) represent the cases of the amplitudes of the chirp signal input of 1, 2, and 3 V respectively

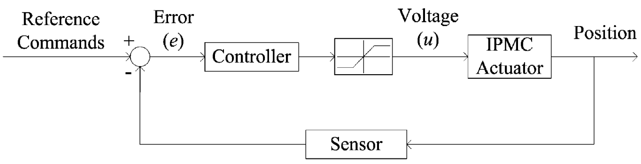

Fig. 7 Schematic diagram of the closed-loop position control of the three-finger gripper. The saturation block was inserted between the controller and the IPMC actuator to protect the IPMC strips from high-voltage damage

The time-domain performance requirements that were attempted are following: the rise time t_r is less than 2.5 s for the step response to reach 90 per cent from 10 per cent of its final value; the settling time t_s is less than 7.5 s for the 5 per cent criterion; and the maximum overshoot M_p is less than 20 per cent. Table 1 summarizes the performance requirements.

The saturation limit for the control input is set to ± 3 V to protect the IPMC strips from high-voltage damage. After tuning the parameters of the discrete-time PID controller, a 60° phase margin could be achieved by adjusting the gain with the Matlab 'rltool'. Note that three independent controllers were designed for each IPMC strip based on its own model. The finalized discrete-time PID controller is

$$C(z) = K_p + \frac{K_i T_s(z+1)}{2(z-1)} + \frac{2K_d(z-1)}{T_s(z+1)(2T(z-1)/(T_s(z+1)+1))} \qquad (3)$$

where $T = 0.01$ s, $T_s = 0.004$ s

$K_p \in [0.39653, 0.56376]$ V/mm

$K_i \in [1.5094, 3.5594]$ V/mm s

$K_d \in [-0.0012895, 0.013129]$ V s/mm

Table 1 Performance requirements of time-domain transient responses

	Design specifications
Maximum overshoot (M_p)	<20%
Settling time (t_s)	<7.5 s (for 5% criterion)
Rise time (t_r)	<2.5 s (from 10% to 90%)

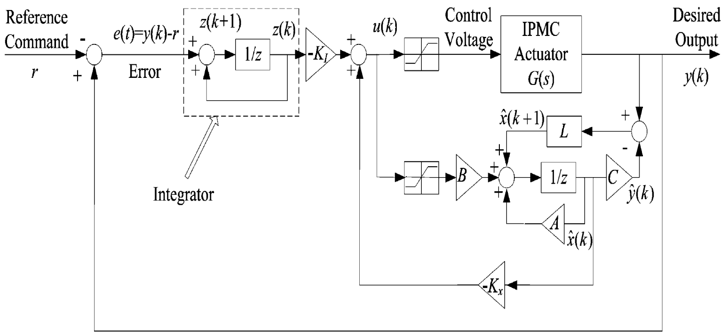

Fig. 8 Schematic diagram of the integrator-augmented closed-loop position control using an LQR with an observer

4.2 Linear quadratic regulation with an observer

A linear time-invariant discrete-time system model for motion control can be represented in state space as

$$\begin{aligned} \boldsymbol{x}(k+1) &= \mathbf{A}\boldsymbol{x}(k) + \mathbf{B}\boldsymbol{u}(k) \\ \boldsymbol{y}(k) &= \mathbf{C}\boldsymbol{x}(k) \end{aligned} \tag{4}$$

where $\boldsymbol{x}$ is the state vector, $\boldsymbol{u}$ is the control input vector, $\boldsymbol{y}$ is the output vector, and $\mathbf{A}$, $\mathbf{B}$, and $\mathbf{C}$ are constant matrices. For the purpose of eliminating the steady-state error, integral states need to be augmented in the controller as shown in Fig. 8.

The augmented system becomes

$$\begin{bmatrix} \boldsymbol{x}(k+1) \\ z(k+1) \end{bmatrix} = \begin{bmatrix} \mathbf{A} & 0 \\ \mathbf{CA} & 1 \end{bmatrix} \begin{bmatrix} \boldsymbol{x}(k) \\ z(k) \end{bmatrix} + \begin{bmatrix} \mathbf{B} \\ \mathbf{CB} \end{bmatrix} \boldsymbol{u}(k) = \begin{bmatrix} 0 \\ -1 \end{bmatrix} r(k) \tag{5}$$

with a new set of variables

$$z(k) = z(k-1) + y(k) - r(k-1)$$

where $r(k)$ is a reference command [**30**]. Let J denote the performance index for the augmented system defined as

$$J = \int_0^\infty (x^{\mathrm{T}} Q x + u^{\mathrm{T}} R u)\, \mathrm{d}t \tag{6}$$

The optimal gain matrix $\mathbf{K}$ for a linear discrete-time system with this quadratic cost function was derived from the algebraic Riccati equation with $Q = qC^{\mathrm{T}}C = \mathrm{diag}(0.001 \times [1 \quad 1 \quad 1 \quad 1])$ and $R = 1$. The control law in Fig. 8 can also be expressed as

$$\boldsymbol{u}(k) = -\mathbf{K}_i z(k) - \mathbf{K}_x \hat{\boldsymbol{x}}(k) \tag{7}$$

where $\mathbf{K} = [K_i \quad K_x] = [0.031\,286 \quad 0.010\,873 \quad 0.019\,098 \quad 0.014\,851 \quad -0.004\,8572]$.

To estimate unavailable velocity states and keep the closed-loop system stable, the eigenvalues of the matrix $(\mathbf{A} - \mathbf{LC})$ must be placed inside the unit circle using the observer gain matrix $\mathbf{L}$. The eigenvalues should also be faster than the closed-loop eigenvalues of the system, as specified by the state feedback gain matrix $\mathbf{K}$. Faster eigenvalues imply a smaller magnitude for these eigenvalues, i.e. closer to the origin of the z plane. The observer poles were selected to be 10 times faster than the controller poles and $\mathbf{L}$ was calculated to be $[25.993\,373 \quad 53.205\,025 \quad 25.566\,189 \quad 0.014\,851 \quad 0.419\,645]$.

5 SIMULATION AND EXPERIMENTAL RESULTS

Manipulation tasks require precise position information of the end-effector in the reference frame. With advanced fabrication techniques it might be possible to fabricate microtips to build on to the

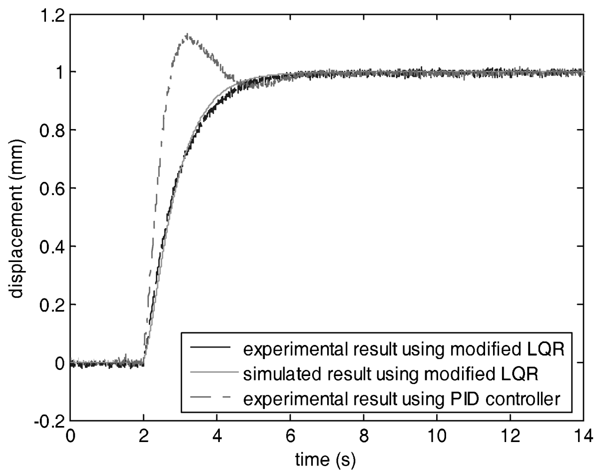

Fig. 9 Step responses of 1 mm with a simulated result (solid line), an experimental result (dashed line) using the modified LQR, and an experimental result (dash–dotted line) using the PID controller

fingers of the microgripper. Then the same microgripper system could be used for the manipulation of nano-sized objects such as carbon nanotubes. This system should be made modular so that it can interface with other manipulation platforms like a microrobot. The present gripper has three fingers, which gives more flexibility to the design. The gripper fingers are made of IPMCs, which along with the position feedback of the actuator will help in developing a force feedback mechanism for a human–machine interface device such as a joystick. In the rest of this section, key simulation and experimental results using the developed microgripper are presented.

5.1 Step responses with PID and LQR controllers

Figure 9 shows 1 mm closed-loop position step responses of an IPMC strip, comparing the performances of the PID controller and the modified LQR (linear quadratic regulator). Although there were uncertainties in the approximated linear model,

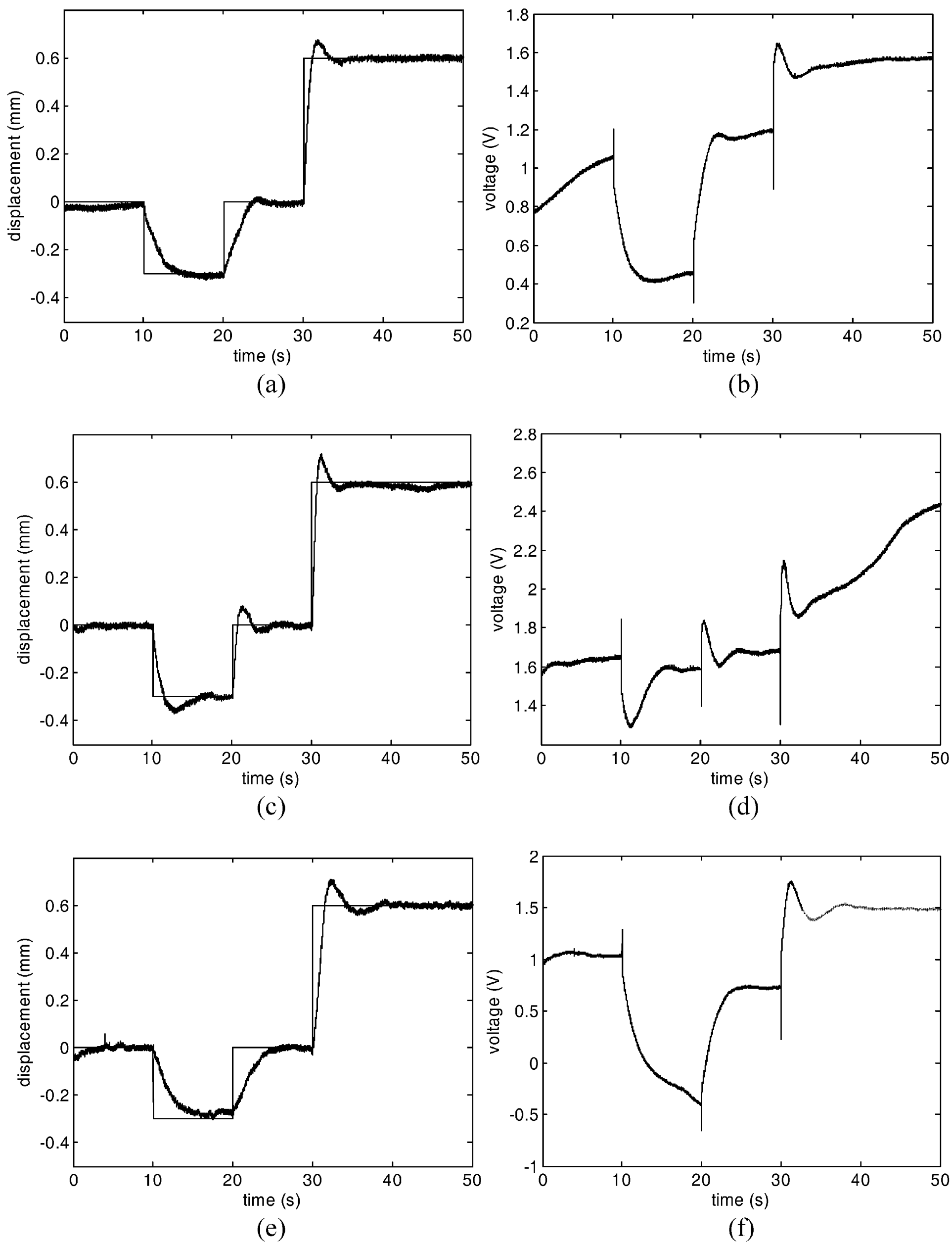

Fig. 10 (a) −0.3 and 0.6 mm step responses and (b) the control input voltage of IPMC finger 1; (c) and (d) of IPMC finger 2; (e) and (f) of IPMC finger 3

the 1 mm step response using the modified LQR matched well in both simulation and experiment, as shown in Fig. 8. Since the control input voltage was below the saturation limit, ± 3 V, the IPMC actuator could track the desired position without causing instability. As shown in Fig. 9, the settling time decreased to 2.85 from 2.98 s, and the overshoot decreased to 1.96 from 14.06 per cent. The steady state error was eliminated in both cases, which is very important when manipulating the microactuator effectively in the 'pick-and-place' operations. The achieved time-domain transient responses shown in Fig. 9 are summarized in Table 2.

5.2 Macroscale motion control

Figure 10 shows the tracking performance of the three IPMC fingers with respect to the given position command profiles. The IPMC gripper was initialized in the first 10 s. After that the control voltage

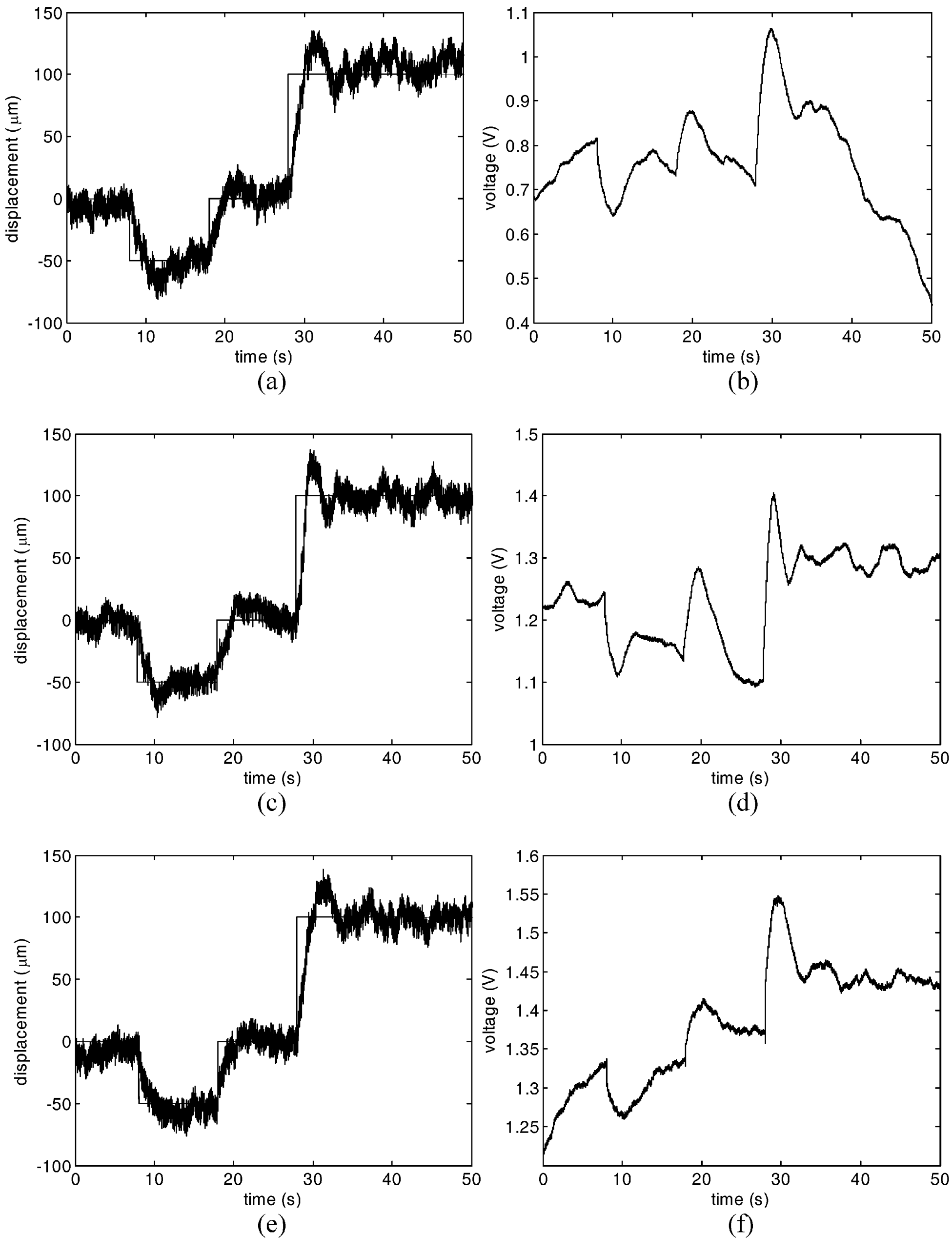

Fig. 11 (a) -50 and 100 μm step responses and (b) the control input voltage of IPMC finger 1; (c) and (d) of IPMC finger 2; (e) and (f) of IPMC finger 3

Table 2 Achieved time-domain transient responses

	PID controller	LQR with observer
Maximum overshoot (M_p)	14.06%	1.96%
Settling time (t_s)	2.98 s	2.85 s
Rise time (t_r)	0.56 s	1.87 s

generated a bending motion to reach the first commanded position profile that simulated picking up a small object until the gripper moved to the target place. When the object reached the target place, the gripper started to release the object. Figures 10(a) and (b) indicate the closed-loop position response and the control input voltage of IPMC finger 1 respectively. Figures 10(c) and (d) are of IPMC finger 2 and Figs 10(e) and (f) are of IPMC finger 3 in the same order.

5.3 Microscale motion control

The developed three-finger gripper has significant potential to be used as a micro- and nano-manipulation device. Figure 11 shows −50 and

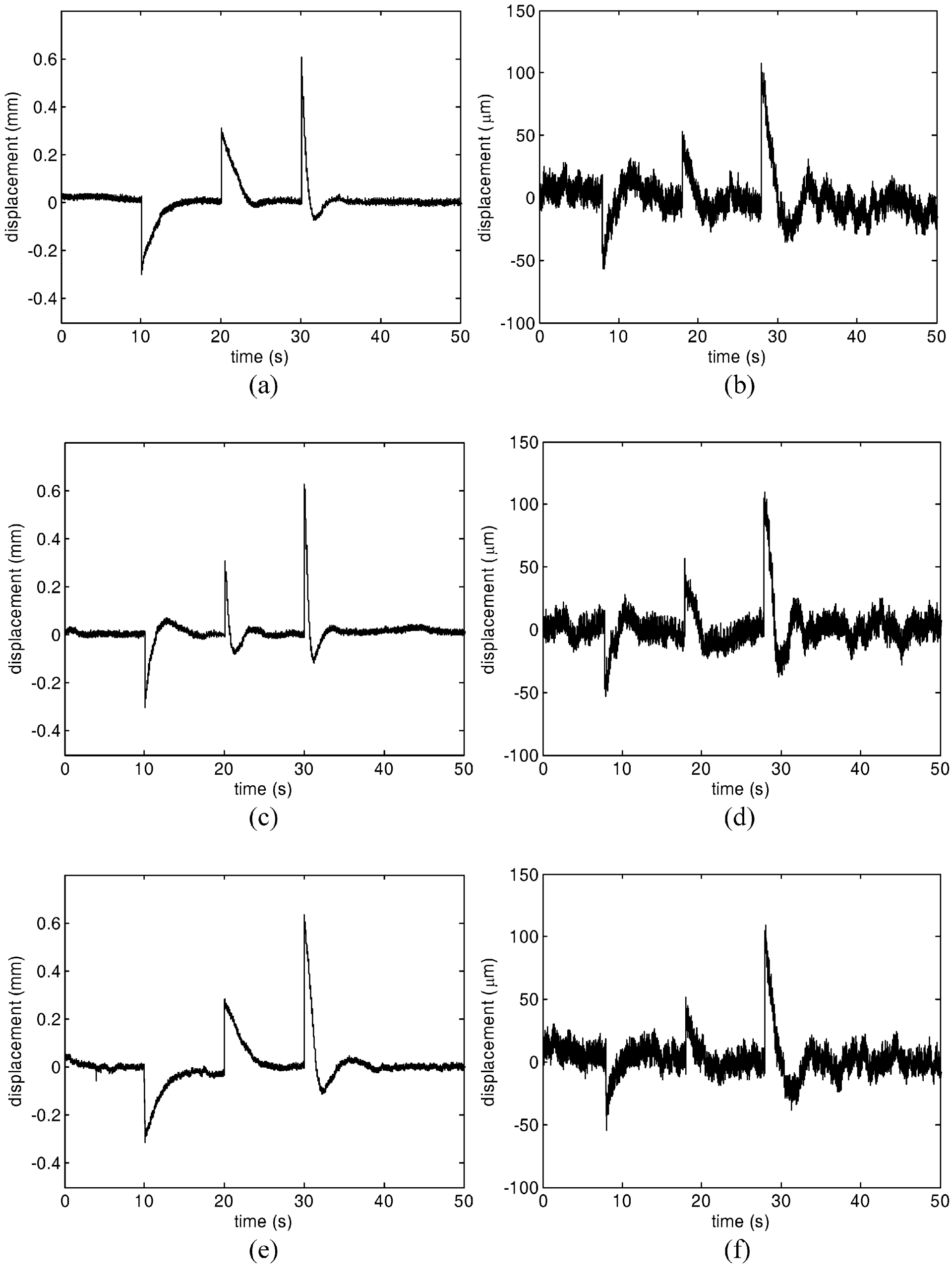

Fig. 12 (a), (c), and (e) errors in the −0.3 and 0.6 mm step responses of IPMC fingers 1, 2, and 3 respectively and (b), (d), and (f) errors in the −50 and 100 μm step responses of IPMC fingers 1, 2, and 3 respectively

100 μm closed-loop step responses and the corresponding control voltage inputs. Since the control inputs were well within the safe operation range of ± 3 V, no integrator antiwindup was necessary [**27**]. The difference between the minimum and maximum control voltages was only about 0.7 V in Figs 11(b), (d), and (f). For the errors corresponding to the given position command profiles, Figs 12(a), (c), and (e) show errors in the -0.3 and 0.6 mm step responses of IPMC fingers 1, 2, and 3 respectively and Figs 12(b), (d), and (f) show errors in the -50 and 100 μm step responses of IPMC fingers 1, 2, and 3 respectively. Each peak occurs due to sudden changes from different step inputs.

5.4 Additional control response

The gripper's time-domain performance in response to another standard test signal, a ramp input, is provided in Fig. 13. The tracking error approaches zero

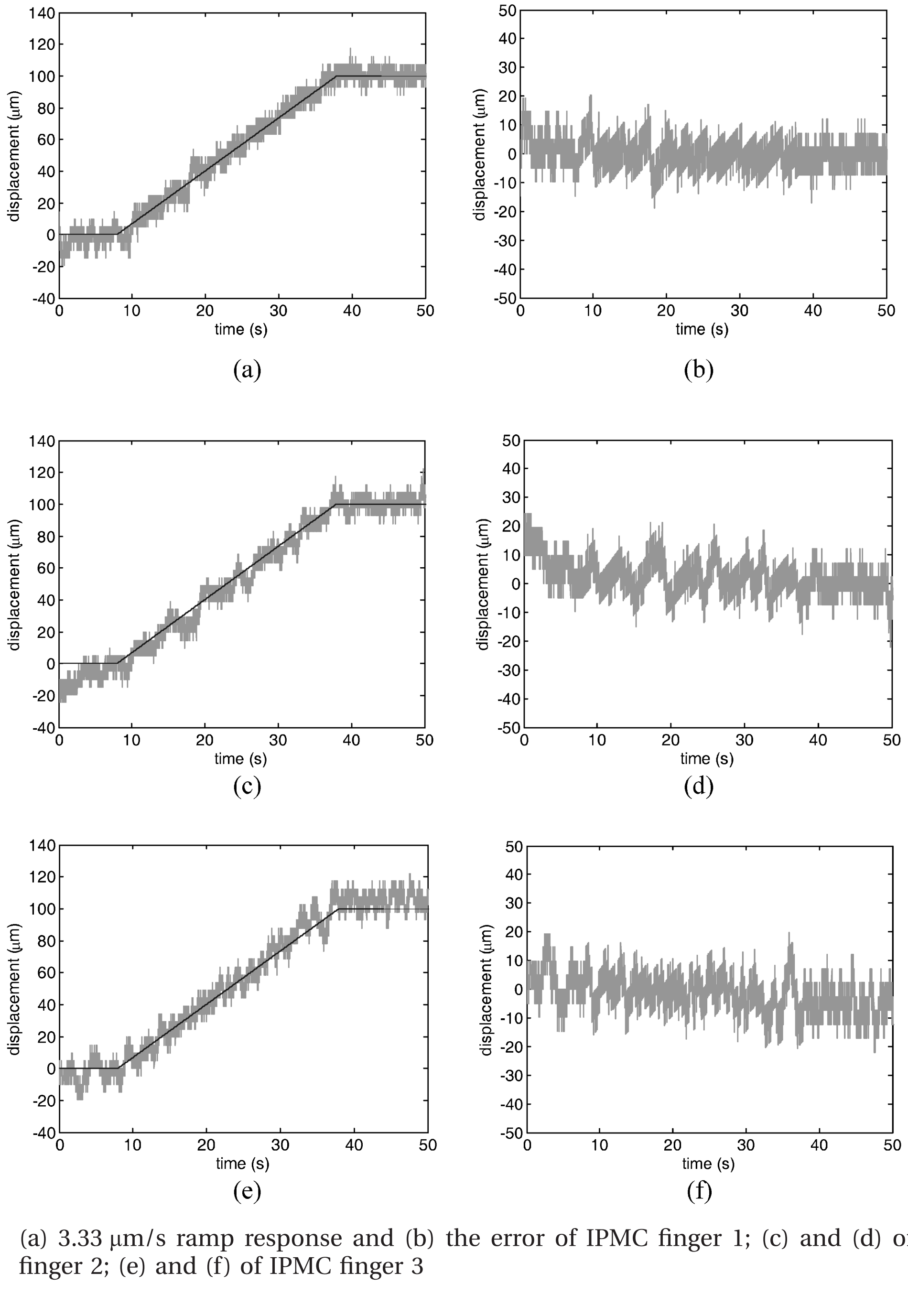

Fig. 13 (a) 3.33 μm/s ramp response and (b) the error of IPMC finger 1; (c) and (d) of IPMC finger 2; (e) and (f) of IPMC finger 3

even if the output follows a non-decaying command. As shown in Fig. 13, the IPMC gripper was regulated for initialization in the first 8 s. After the ramp reference signal was applied, appropriate control voltages were generated to follow the command trajectory. The ramp command trajectory went from 0 to 100 μm in 30 s. Figure 13(a) and (b) represent the closed-loop response to the ramp command profile with a slope of 3.33 μm/s and the tracking error of IPMC finger 1 respectively. Figures 13(c) and (d) are of IPMC finger 2 and Figs 13(e) and (f) are of IPMC finger 3 in the same order. The mean values of the errors are −0.1281, 2.7979, and −4.7891 μm with the standard deviations of 5.2788, 8.3575, and 8.4697 μm in the order of IPMC fingers 1, 2, and 3.

6 CONCLUSIONS

In this paper, a three-finger IPMC gripper's dynamic behaviour was discussed. A linear model for the IPMC using a chirp signal with 1, 2, and 3 V amplitudes in the interesting frequency range of (0.62 Hz, 5 Hz) for the system identification was developed. The Bode plots of the system transfer functions obtained from a PSD analysis and a BJ model matched well within the interesting frequency range. It was observed that FFT magnitudes of the peak measured displacements obtained from the experimental outputs were linearly decreased by about 0.0035 mm s with respect to decreasing the voltage amplitude by 1 V from 3 V.

A classical PID controller and a modified LQR controller to enhance the system dynamics and their transient response performance were designed, implemented, and verified by simulation and experiment. In an experimental case of a 1 mm step response in the closed-loop system, the maximum overshoot was reduced from 14.06 to 1.96 per cent without increasing the settling time using a modified LQR controller compared with the performance using a PID controller. However, the rise time of the LQR controller is about three times as long as that of the PID controller. The accomplished zero steady-state error was crucial to manipulate the IPMC actuator effectively in 'pick-and-place' operations.

The linear approximation of inherently non-linear IPMC dynamics was suitable for the microscale gripping application since the control voltage was below the saturation limit. The precise manipulation of this three-finger gripper was successfully demonstrated with experimental closed-loop responses in both the macroscale and microscale.

ACKNOWLEDGEMENTS

The authors would like to thank Dr Donald Leo and Mr Matt Bennett of Virginia Polytechnic Institute and State University for providing them with IPMC samples.

REFERENCES

1 **Nemat-Nasser, S.** and **Wu, Y.** Comparative experimental study of ionic polymer-metal composites with different backbone ionomers and in various cation forms. *J. Appl. Physics*, May 2003, **93**, 5255–5267.
2 **Shahinpoor, M.** and **Kim, K. J.** The effect of surface-electrode resistance on the performance of ionic polymer–metal composite (IPMC) artificial muscles. *Smart Mater. Structs*, August 2000, **9**, 543–551.
3 **Shahinpoor, M.** and **Kim, K. J.** Experimental study of ionic polymer–metal composites in various cation forms: actuation behavior. *Sci. Engng of Composite Mater.*, 2002, **10**, 423–436.
4 **Paquette, J. W., Kim, K. J.,** and **Kim, D.** Low temperature characteristics of ionic polymer–metal composite actuators. *Sensor and Actuators A – Physical*, January 2002, **118**, 135–143.
5 **Kim, S. J., Kim, M. S., Shin, S. R., Kim, I. Y., Kim, S. I., Lee, S. H., Lee, T. S.,** and **Spinks, G. M.** Enhancement of the electromechanical behavior of IPMCs based on chitosan/polyaniline ion exchange membranes fabricated by freeze-drying. *Smart Mater. Structs*, October 2005, **14**, 889–894.
6 **Kim, K. J.** and **Shahinpoor, M.** A novel method of manufacturing three-dimensional ionic polymer–metal composites (IPMCs) biomimetic sensors, actuators and artificial muscles. *Polymer*, February 2002, **43**, 797–802.
7 **Shahinpoor, M.** and **Kim, K. J.** Ionic polymer–metal composite: I. Fundamentals. *Smart Mater. Structs*, August 2001, **10**, 819–833.
8 **Tamagawa, H., Yagasaki, K.,** and **Nogata, F.** Mechanical characteristics of ionic polymer–metal composite in the process of self-bending. *J. Appl. Physics*, December 2002, **92**, 7614–7618.
9 **Lee, S., Park, H. C.,** and **Kim, K. J.** Equivalent modeling for ionic polymer–metal composite actuators based on beam theories. *Smart Mater. Structs*, December 2005, **14**, 1363–1368.
10 **Park, H. C., Lee, S.,** and **Kim, K. J.** Equivalent modeling for shape design of IPMC (ionic polymer–metal composite) as flapping actuator. *Key Engng Mater.*, November 2005, **297–300**, 616–621.
11 **Dimarogonas, A. D.** and **Haddad, S. D.** *Vibration for engineers*, 1992 (Prentice-Hall, Englewood Cliffs, New Jersey).
12 **Nemat-Nasser, S.** and **Li, J. Y.** Electromechanical response of ionic polymer metal composites. *J. Appl. Physics*, April 2000, **87**, 3321–3331.

13 **Kanno, R., Tadokoro, S., Takamori, T.,** and **Hattori, M.** Linear approximate dynamic model of ICPF (ionic conducting polymer gel film) actuator. In Proceedings of the IEEE International Conference on *Robotics and automation*, April 1996, pp. 219–225.
14 **Shahinpoor, M.** Mechanoelectrical phenomena in ionic polymers. *Mathematics and Mechanics of Solids*, June 2003, **8**, 281–288.
15 **Paquette, J. W., Kim, K. J., Nam, J.-D.,** and **Tak, Y. S.** An equivalent circuit model for ionic polymer–metal composites and their performance improvement by a clay-based polymer nano-composite technique. *J. Intell. Mater. Systems Structs*, October 2003, **14**, 633–642.
16 **Paquette, J. W., Kim, K. J., Kim, D.,** and **Yim, W.** The behavior of ionic polymer–metal composites in a multi-layer configuration. *Smart Mater. Structs*, October 2005, **14**, 881–888.
17 **Kim, B., Kim, D.-H., Jung, J.,** and **Park, J.-O.** A biomimetic undulatory tadpole robot using ionic polymer–metal composite actuators. *Smart Mater. Structs*, December 2005, **14**, 1579–1585.
18 **Bonomo, C., Fortuna, L., Giannone, P.,** and **Graziani, S.** A circuit to model the electrical behavior of an ionic polymer–metal composite. *IEEE Trans. Circuit and Systems*, February 2006, **52**, 338–350.
19 **Bhat, N.** and **Kim, W.-J.** Precision force and position control of an ionic polymer metal composite. *Proc. Instn Mech. Engrs, Part I: J. Systems and Control Engineering*, September 2004, **218**(I6), 421–432.
20 **Bar-Cohen, Y.** Electroactive polymer as artificial muscles – reality and challenges. In Proceedings of the 42nd AIAA Meeting on *Structural dynamics and materials*, Seattle, USA, 2001, Vol. 1492, pp. 1–9.
21 **Kanno, R., Kurata, A., Hattori, M., Tadokoro, S., Takamori, T.,** and **Oguro, K.** Characteristics and modeling of ICPF actuator. In Proceedings of Japan–USA Symposium on *Flexible automation*, Tokyo, Japan, July 1994, Vol. 2, pp. 691–698.
22 **Kothera, C. S.** and **Leo, D. J.** Identification of the nonlinear response of ionic polymer actuators using the Volterra series. *J. Vibr. and Control*, April 2005, **4**, 519–541.
23 **Kothera, C. S.** and **Leo, D. J.** Bandwidth characterization in the micropositioning of ionic polymer actuator. *J. Intell. Mater. Systems and Structs*, January 2005, **16**, 3–13.
24 **Ewins, D.** *Modal testing: theory and practice*, 1986 (Brüel and Kjær).
25 **Harris, C.** *Shock and vibration handbook*, 1995 (McGraw-Hill, New York).
26 **Tao, G.** and **Ioannou, P. A.** Persistency of excitation and overparameterization in model reference adaptive control. In Proceedings of the 27th Conference on *Decision and control*, Austin, USA, December 1988, pp. 757–758.
27 **Yun, K.** and **Kim, W.-J.** Microscale position control of electroactive polymer using anti-windup scheme. *Smart Mater. Structs*, 2006, **15**(4), 924–930.
28 **Gelb, A.** *Applied optimal estimation*, 1974 (The MIT Press, Cambridge, Massachusetts).
29 *Simulink response optimization toolbox* (The Mathworks, Inc., Natick, Massachusetts).
30 **Gopal, M.** *Digital control and state variable methods*, 2003 (McGraw-Hill, New York).

APPENDIX

Notation

$\mathbf{A}$, $\mathbf{B}$, $\mathbf{C}$	system, input, and output matrices
t_i	the state-space representation of a dynamic system
d_3, d_2, d_1, d_0	denominator coefficients of $G(s)$
$G(s)$	rational transfer function
J	performance index
$\mathbf{K}$	controller gain matrix
K_p, K_i, K_d	proportional gain (V/mm), integral gain (V/mm s), and derivative gain (V s/mm)
l_i	controlled range (mm)
$\mathbf{L}$	observer gain matrix
M_p	overshoot (%)
n_3, n_2, n_1, n_0	numerator coefficients of $G(s)$
Q, R	cost functions
r	radius of object (mm)
t_i	thickness of the three-finger gripper (mm)
t_r	rise time (s)
t_s	settling time (s)
T_s	sampling time (s)
$\boldsymbol{u}(k)$	discrete control input vector (V)
w_i	width of the three-finger gripper (mm)
$\boldsymbol{x}(k)$	discrete state vector
$\boldsymbol{y}(k)$	discrete output vector (mm)
$\boldsymbol{z}(k)$	new set of discrete variables (mm)
$\Phi_{xx}(\omega)$	power spectral density function of the input
$\Phi_{yy}(\omega)$	power spectral density function of the output